Small molecule blockade of transcriptional coactivation of the hypoxia-inducible factor pathway

Andrew L. Kung,[1,2,*] Sonya D. Zabludoff,[3,6] Dennis S. France,[3] Steven J. Freedman,[1,4,7] Elizabeth A. Tanner,[1] Annelisa Vieira,[1] Susan Cornell-Kennon,[3] Jennifer Lee,[3] Beqing Wang,[3] Jamin Wang,[3] Klaus Memmert,[5] Hans-Ulrich Naegeli,[5] Frank Petersen,[5] Michael J. Eck,[1] Kenneth W. Bair,[3,8] Alexander W. Wood,[3] and David M. Livingston[1,*]

[1]Dana-Farber Cancer Institute and Harvard Medical School, Boston, Massachusetts 02115
[2]Department of Pediatric Oncology, Dana-Farber Cancer Institute, and Children's Hospital, Boston, Massachusetts 02115
[3]Novartis Pharmaceuticals Corporation, Oncology Department, Cambridge, Massachusetts 02139
[4]Division of Hematology/Oncology, Beth Israel Deaconess Medical Center, Boston, Massachusetts 02115
[5]Novartis Pharma AG Natural Products Unit/Discovery Technologies, Basel, Switzerland CH-4002
[6]Present address: AstraZeneca, Cancer Discovery, R & D Boston, Waltham, Massachusetts 02451
[7]Present address: Merck Research Laboratories, West Point, Pennsylvania 19486
[8]Present address: Chiron Corporation, Emeryville, California 94608
*Correspondence: andrew_kung@dfci.harvard.edu; david_livingston@dfci.harvard.edu

Summary

Homeostasis under hypoxic conditions is maintained through a coordinated transcriptional response mediated by the hypoxia-inducible factor (HIF) pathway and requires coactivation by the CBP and p300 transcriptional coactivators. Through a target-based high-throughput screen, we identified chetomin as a disrupter of HIF binding to p300. At a molecular level, chetomin disrupts the structure of the CH1 domain of p300 and precludes its interaction with HIF, thereby attenuating hypoxia-inducible transcription. Systemic administration of chetomin inhibited hypoxia-inducible transcription within tumors and inhibited tumor growth. These results demonstrate a therapeutic window for pharmacological attenuation of HIF activity and further establish the feasibility of disrupting a signal transduction pathway by targeting the function of a transcriptional coactivator with a small molecule.

Introduction

Signal transduction pathways translate extracellular signals and environmental stimuli into changes in the gene expression profile of cells. In cancer, many oncogenic changes deregulate signal transduction pathways (Darnell, 2002). Additionally, signal transduction pathways also play key roles in maintaining tumor cell homeostasis, for example, adaptation to hypoxia by induction of hypoxia-inducible factor (HIF) and expression of vascular endothelial growth factor (VEGF) (Huang and Bunn, 2003; Pugh and Ratcliffe, 2003; Semenza, 2002). Efforts to target key components of signal transduction pathways have resulted in therapeutic successes, most often through inhibition of receptors or upstream signal mediators. For example, trastuzumab, imatinib mesylate, and rituximab, exemplars of the modern paradigm of targeted therapies, all target cell surface receptors. There are few examples of success in targeting downstream mediators of signal transduction, such as activated transcription factors or transcriptional complexes.

Hypoxia is an almost universal hallmark of solid tumors (Vaupel et al., 1998; Zhong et al., 1999). Adaptation to hypoxia is critical for tumor survival and growth and is mediated in large part by transcriptional activation of genes that facilitate short-term adaptive mechanisms (e.g., increased vascular permeability, vasodilatation, glucose transport, switch to anaerobic metabolism), as well as long-term adaptive mechanisms (e.g., angiogenesis) (Harris, 2002; Huang and Bunn, 2003; Pugh and Ratcliffe, 2003; Semenza, 2002). This coordinated homeostatic response is mediated in large part through the activation of the heterodimeric transcription factor hypoxia-inducible factor 1 (HIF-1). Tumor hypoxia and overexpression of HIF-1 have been associated with resistance to certain therapies, increased risk of invasion and metastasis, and poor outcome in certain malignancies (Hockel and Vaupel, 2001).

SIGNIFICANCE

Adaptation to hypoxia is critical for tumor growth. In this report, we describe our efforts to find a small molecule capable of disrupting the HIF pathway by blocking the interaction of HIF with its transcriptional coactivator, p300. Although the interaction surface between these two proteins is extensive, we identify a small molecule that abrogates binding by disrupting the structure of one of the binding partners. These results demonstrate the feasibility of nonallosteric small molecule perturbation of high-affinity protein-protein interactions. Furthermore, they show that signal transduction pathways can be attenuated by impinging upon downstream pathway constituents, such as the function of a transcriptional coactivator. This strategy may be relevant to other signal transduction pathways aberrantly activated in cancer.

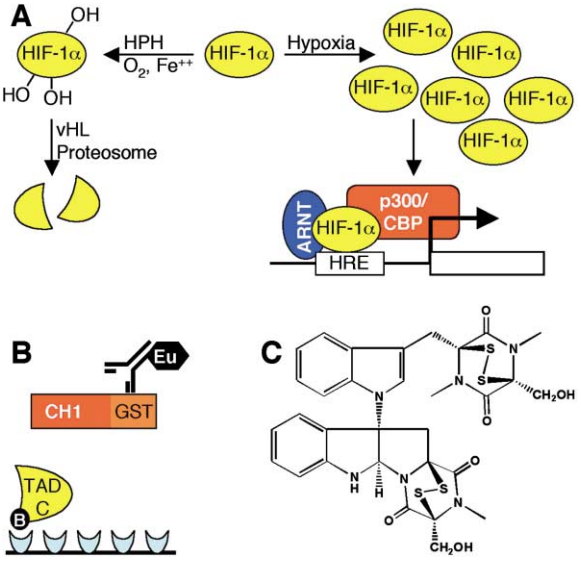

Figure 1. HTS for disrupters of HIF-1α/p300 binding

A: Schematic of HIF-1 hypoxia response pathway.
B: Time-resolved fluorescence HTS for inhibitors of HIF-p300 binding. Biotinylated HIF-1α polypeptide (TADC) was immobilized on streptavidin plates. In the presence of compounds, the binding of bacterially produced GST-CH1 was probed with a europium (Eu)-conjugated anti-GST antibody.
C: Structure of chetomin.

Many of the mechanisms that regulate the HIF-1 pathway have been recently elucidated (Figure 1A). Under conditions of normal oxygenation, the regulated α-subunit (HIF-1α) is hydroxylated on prolines 402 and 564 in oxygen-dependent reactions, targeting HIF-1α to the von Hippel-Lindau (vHL) ubiquitination complex and ultimate degradation by the proteasome system (Huang et al., 1998; Ivan et al., 2001; Jaakkola et al., 2001; Kallio et al., 1999; Masson et al., 2001). In this manner, HIF-1α abundance is maintained at nominal levels under normoxic conditions. As oxygen becomes rate limiting, proline hydroxylation diminishes, and HIF-1α accumulates and heterodimerizes with the constitutively present β-subunit (HIF-1β, aryl hydrocarbon nuclear translocator) (Huang and Bunn, 2003; Pugh and Ratcliffe, 2003). A third site of regulatory hydroxylation on asparagine 803 is also inhibited under hypoxic conditions, allowing for recruitment of the p300 and CREB binding protein (CBP) transcriptional coactivators (Lando et al., 2002). Binding of this complex to the cognate hypoxia-response element (HRE) results in transactivation of genes containing such elements within promoter or enhancer elements (Semenza, 2002).

The near universality of hypoxia in human tumors and centrality of the HIF pathway in adapting to hypoxia suggests that inhibition of the HIF pathway may have therapeutic utility as an antitumor strategy. Inhibition of HIF function in tumors may attenuate angiogenesis and may contribute directly to tumor cell death through metabolic derangement. While some experimental xenograft studies support targeting the HIF pathway as an antitumor strategy (Kondo et al., 2002; Kung et al., 2000), other mouse genetic experiments have had conflicting results (Carmeliet et al., 1998; Hopfl et al., 2002; Ryan et al., 1998, 2000), thus necessitating caution as this strategy is translated to clinical utility.

A number of strategies to preferentially target hypoxic tumor cells have been devised. The first to achieve clinical utility has been the development of drugs that have heightened toxicity under hypoxic conditions, for example, tirapazamine, a hypoxia-activated topoisomerase II inhibitor (von Pawel et al., 2000). Experimental approaches include gene therapy constructs containing HREs that drive expression under hypoxic conditions and prodrug activation by obligate anaerobic microbes (Brown, 2002). Additionally, recent reports have identified inhibition of the HIF pathway by antimicrotubule agents (Mabjeesh et al., 2003), topoisomerase inhibitors (Rapisarda et al., 2002), histone deacetylase inhibitors (Mie Lee et al., 2003), and HSP90 inhibitors (Hur et al., 2002; Isaacs et al., 2002; Mabjeesh et al., 2002), although the specificity of these effects and relevance vis-à-vis their antitumor activities in vivo is not clear.

We and others have previously shown that p300 and CBP are critical coactivators of the HIF-1 pathway (Arany et al., 1996; Carrero et al., 2000; Ema et al., 1999; Kung et al., 2000). Disrupting the normal interaction of p300/CBP with HIF-1α by retroviral overexpression of a blocking polypeptide resulted in diminished hypoxia-inducible transcription and decreased tumor growth in xenograft models (Kung et al., 2000). While these approaches provide experimental support for the importance of the HIF pathway in tumorigenesis, therapeutic delivery of moderate-sized blocking polypeptides is not readily feasible. Although pharmacological manipulation of nuclear protein-protein interactions has proven difficult (Cochran, 2000), there have been a limited number of recent successes (Berg et al., 2002; Lepourcelet et al., 2004). Here, we describe a target-based screen that identified a small molecule inhibitor of the interaction of HIF-1 with p300. We demonstrate that the small molecule attenuates hypoxia-inducible transcription in cell culture, as well as within tumor xenografts, and has antitumor efficacy in vivo.

Results

High-throughput screen for disrupters of HIF-1α/p300 binding

We developed a high-throughput screen (HTS) to search for small molecules capable of disrupting the interaction of HIF-1α with p300 (Figure 1B). A biotinylated, 41 amino acid polypeptide corresponding to the minimal p300/CBP binding domain of HIF-1α (TADC; residues 786-826 [Kung et al., 2000]) was synthesized and immobilized on streptavidin-coated multiwell plates. The minimal HIF-1α binding domain of p300 (CH1; residues 302-423 [Kung et al., 2000]) was produced in bacteria as a fusion to glutathione-S-transferase (GST-CH1). Binding of GST-CH1 to immobilized TADC, in the presence or absence of compounds, was probed by europium-conjugated anti-GST antibody and detected by time-resolved fluorescence. The optimized HTS assay had an average signal-to-noise ratio of greater than 5:1 and a very robust assay quality parameter Z′ factor value (Zhang et al., 1999) of 0.82.

A natural and synthetic compound library of >600,000 substances was subjected to this HTS. Compounds with >50% inhibitory activity were titrated to determine a dose-response relationship (7 point IC_{50}). Due to the high binding affinity of these polypeptides (Freedman et al., 2002, 2003), the hit rate was low. There were only 187 titrated hits (0.03% titrated hit rate), which were then subjected to secondary assays consisting of an in vitro interaction assay of full-length HIF-1α with GST-

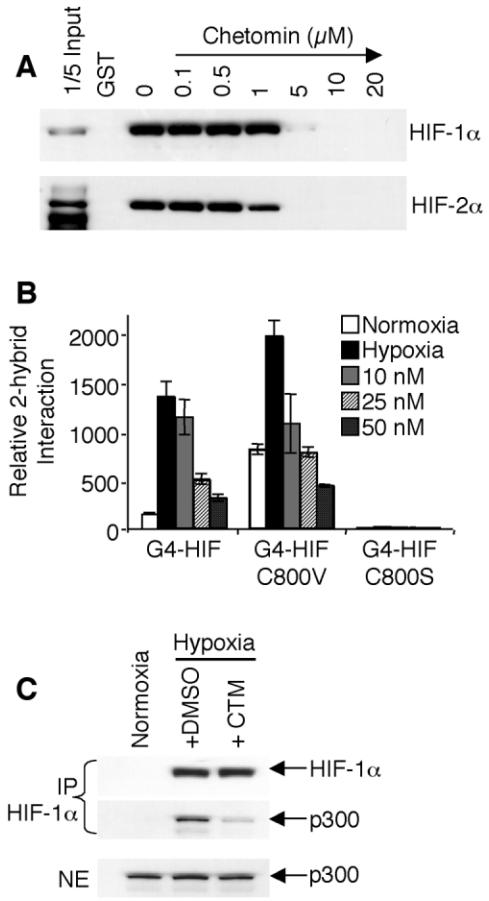

Figure 2. Chetomin disrupts HIF-1α and HIF-2α binding to p300

A: In vitro interaction assay. Full-length IVT HIF-1α and HIF-2α were bound to GST-CH1 in the absence or presence of chetomin at the indicated concentrations or to GST as a negative control.

B: Mammalian two-hybrid interaction assay. Hep3B cells were cotransfected with VP16-CH1 and the indicated Gal4-fusion of HIF-1α (G4-HIF), an interacting mutant (G4-HIF-C800V), or a noninteracting mutant (G4-HIF-C800S). Relative two-hybrid interaction was determined under normoxic or hypoxic conditions and in the absence or presence of the indicated concentrations of chetomin. Reporter activity is normalized to an internal transcriptional control (β-galactosidase activity) and expressed as the average of triplicates ± SD.

C: Interaction of endogenous HIF-1α and p300. HepG2 cells were treated with 50 nM chetomin (CTM) or solvent (DMSO) under normoxic or hypoxic conditions. HIF-1α was immunoprecipitated (IP HIF-1α) from normalized aliquots of nuclear extract, and HIF-1α and p300 were detected by immunoblot. Cellular abundance of p300 was determined by immunoblot of 50 μg of unfractionated nuclear extract (NE).

CH1 (see Figure 2A) and a cell-based assay utilizing the hypoxia-responsive erythropoietin (EPO) enhancer driving luciferase (see Figure 4A). From this HTS and secondary analyses, a single submicromolar inhibitor or HIF-1α/p300 interaction, chetomin (Figure 1C), was identified.

Chetomin, a dithiodiketopiperazine metabolite of the fungus *Chaetomium* species, has been previously characterized as having antimicrobial activity (Brewer et al., 1972; Sekita et al., 1981). Complete synthesis of chetomin has not been achieved, and as such the compound used for subsequent studies was produced by fermentation, followed by organic extraction, and purification by silica gel and reverse phase C18 chromatography. The molecular formula of the compound was determined by high-resolution mass spectroscopy (ESI; 9.4 Tesla FT/MS) to be $C_{31}H_{30}N_6O_6S_4$ (observed m/z $[M+H]^+$ 711.1182; calculated m/z 711.1182; rel. error < 0.1 ppm; data not shown). NMR spectroscopy ($CDCl_3$; 500 MHz; tetramethylsilane as internal standard) revealed that all ^1H and ^{13}C shifts (Supplemental Figure S1 at http://www.cancercell.org/cgi/content/full/6/1/33/DC1) corresponded with those published for chetomin (Fujimoto et al., 2004; McInnes et al., 1976). The optical rotation $[\alpha]_D^{23}$ was $+283.2°$ ($c = 0.101$ in chloroform; data not shown), which was likewise consistent with the published data of chetomin (Fujimoto et al., 2004), confirming the absolute stereochemistry as indicated (Figure 1C). The final purity of chetomin used for these studies was >98% by HPLC analysis.

Chetomin disrupts HIF-1α and HIF-2α binding to p300

The structural elements that are required for HIF-1α binding to p300 are largely identical in HIF-2α (Freedman et al., 2002). We evaluated the ability of chetomin to disrupt binding of HIF-1α and HIF-2α to p300 in an in vitro interaction assay. Full-length in vitro-translated HIF-1α and HIF-2α bound efficiently to GST-CH1 (Figure 2A). Addition of chetomin disrupted binding of both HIF-1α and HIF-2α at similar concentrations.

In cell culture, the interaction of the TADC domain of HIF-1α with the CH1 domain of p300 was evaluated using a mammalian two-hybrid assay. Here, the interaction of CH1 (p300 aa 311-528) fused to the VP16 activation domain (VP16-CH1) and the TADC domain of HIF-1α (aa 776-826) fused to the Gal4 DNA binding domain (Gal4-TADC) was measured in Hep3B cells. The hypoxia-induced interaction between TADC and CH1 was attenuated in a dose-dependent manner by chetomin over a low nanomolar range (Figure 2B). Prior studies have demonstrated a critical requirement for Cys800 within the TADC domain for binding to p300 (Ema et al., 1999; Gu et al., 2001). Covalent attack of Cys800 in TADC by chetomin was excluded as a possible mechanism of action, since chetomin was equally efficacious against a Cys800Val mutant of TADC (Figure 2B) that has been previously reported to bind CH1 with heightened affinity (Gu et al., 2001). There were significant differences in chetomin doses required to disrupt HIF-1α/CH1 interaction in vitro (Figure 2A) compared to in cells (Figure 2B), which we attribute to the microgram quantities of GST-CH1 used in the in vitro interaction assays, in comparison to normal intracellular concentrations of the relevant proteins.

To determine if chetomin disrupted the interaction of endogenous HIF-1α with p300, endogenous HIF-1α was immunoprecipitated from cells, and coimmunoprecipitated p300 was detected by immunoblot. As expected, under normoxic conditions the abundance of HIF-1α is nominal (Figure 2C). Under hypoxic conditions, HIF-1α is readily detectable and exists in complex with p300. While chetomin had no appreciable effect on abundance of HIF-1α or p300 under hypoxic conditions, the abundance of p300 complexed with HIF-1α was significantly reduced upon treatment with chetomin (Figure 2C). Thus, chetomin disrupts p300/HIF-1α protein-protein interaction in vitro and within cells.

Chetomin disrupts CH1 structure/function

To test whether chetomin globally disrupts p300 function, we evaluated the transcriptional activity of proteins binding to various domains of p300. The p300 binding domain of each protein

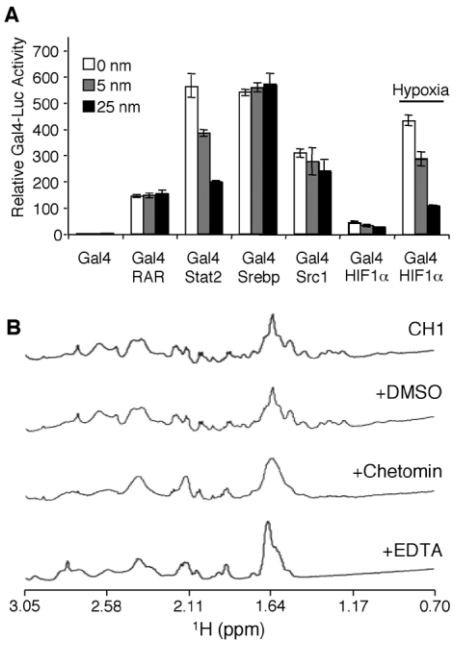

Figure 3. Chetomin disrupts the structure and function of CH1

A: Transactivation of p300-interacting proteins. The DNA binding domain of Gal4 was fused to the p300 binding domain of the indicated proteins. The effect of chetomin on p300-mediated transcription is expressed as luciferase activity normalized to an internal control for transcription. Where indicated, cells were exposed to hypoxia.

B: Effect of chetomin on CH1 structure. One-dimensional proton NMR spectra in the absence (CH1) or presence of solvent alone (DMSO), chetomin, or EDTA. Only the upfield alipathic region is shown.

was fused to the Gal4 DNA binding domain. p300-dependent transcriptional activity was assayed as activity from a Gal4-luciferase reporter. Chetomin had no significant effect on RAR, SREBP2, or SRC-1 transcriptional activity (Figure 3A), demonstrating that chetomin did not globally inhibit p300 activity, as these factors bind to the amino-terminal, KIX, and glutamine-rich domains, respectively. STAT2 transcriptional activity, however, was significantly attenuated by chetomin, in a manner parallel to HIF-1α. Since STAT2 also binds to the CH1 domain (Bhattacharya et al., 1996), these data suggest that chetomin disrupts CH1 function but not p300 function in entirety. These results also demonstrate that chetomin is not a nonspecific transcriptional inhibitor.

To more directly probe the effect of chetomin on CH1, we used NMR spectroscopy to determine the effect of chetomin on the structure of CH1 (Figure 3B). Addition of a 2-fold molar excess of chetomin to HIF-1α in complex with CH1 did not alter the 1D proton NMR spectrum (data not shown). In contrast, the same amount of chetomin added to the CH1 domain alone caused a loss of proton peak dispersion (i.e., the range over which peaks are present) and broadening of spectral linewidths (i.e., the widths of the peaks that are present). These changes indicate that CH1 becomes less structured in the presence of chetomin because spectral complexity is reduced when amino acids become exposed to a uniform solute environment. This is further supported by the chetomin-induced disappearance of amide proton peaks (i.e., centered around 8.35 ppm; data not shown) in a D_2O-containing solvent. Here, when amino acids are not protected from solvent exposure by the structural fold, exchangeable amide protons are rapidly replaced by deuterium ions, which do not have a NMR signal. Lower concentrations of chetomin delayed the onset of change and/or produced only a partial effect, and solvent alone (DMSO) had no effect on the NMR spectrum. Spectral changes observed with chetomin were similar to those caused by EDTA-mediated chelation of zinc ions coordinated by CH1 (Figure 3B), which is known to disrupt its structure (Freedman et al., 2002). Mass spectroscopy demonstrated that chetomin does not covalently modify the CH1 domain or the HIF-1α peptide (data not shown). Taken together, these findings indicate that chetomin targets the CH1 domain of p300, disrupting its global fold and thereby preventing interaction with HIF-1α, as well as other CH1-interacting proteins.

Chetomin attenuates hypoxia-inducible transcription

Having determined that chetomin disrupts binding of HIF to p300, we wanted to determine if chetomin attenuated hypoxia-inducible transcription. Utilizing three hypoxia-responsive reporters in cell-based assays, chetomin was found to attenuate hypoxia-induced reporter activity at low nanomolar concentrations (Figure 4A). All luciferase values were normalized to the CMV-driven expression of β-galactosidase as an internal control. At the indicated concentrations, there was no significant alteration of CMV promoter-driven luciferase activity (Figure 4A), which indicates that chetomin was not directly perturbing the activity of luciferase. These effects were also not due to nonspecific transcriptional repression or cytotoxicity, since standardization to an internal control would correct for decreased overall cell numbers. Furthermore, there was no appreciable decrease in cell viability in HCT116, Hep3B, or human umbilical vein endothelial cells when grown in chetomin up to concentrations of 250 nM for 24 hr (data not shown).

To further verify effects on hypoxia-inducible transcription, real-time RT-PCR was used to quantify the abundance of a panel of hypoxia-induced transcripts. Here too, chetomin reduced the abundance of multiple hypoxia-induced transcripts, albeit with varying efficacy (Figure 4B).

VEGF is a primary mediator of vascular permeability and angiogenesis, and its production is induced by hypoxia (Figures 4C and 4D). Cellular abundance (Figure 4C) as well as supernatant levels of secreted VEGF (Figure 4D) protein were both attenuated by addition of chetomin in a dose-dependent manner. Taken together, these results demonstrate that chetomin attenuates hypoxia-inducible gene expression in cell culture and is not a global inhibitor of transcription at the concentrations that were used in these studies.

Chetomin attenuates HIF pathway function in vivo

When chetomin was administered intravenously in mice, 2 mg/kg was the maximally tolerated single dose. Pharmacokinetic analysis revealed variable peak plasma levels of 1375 $\pm$ 1020 nM that were achieved immediately after injection, with an elimination half-life of 4 hr. Peak xenograft tumor levels were achieved 4 hr after a single intravenous dose, with peak tumor concentration of 300 nM (data not shown).

To determine if chetomin affected HIF-1 pathway in vivo, we first determined the effect of chetomin on serum EPO levels, as a biomarker of physiological HIF-1 function (Semenza, 2002). Mice were treated either with three daily doses of chetomin at 2 mg/kg i.v. or with vehicle control. Serum was collected 6 hr

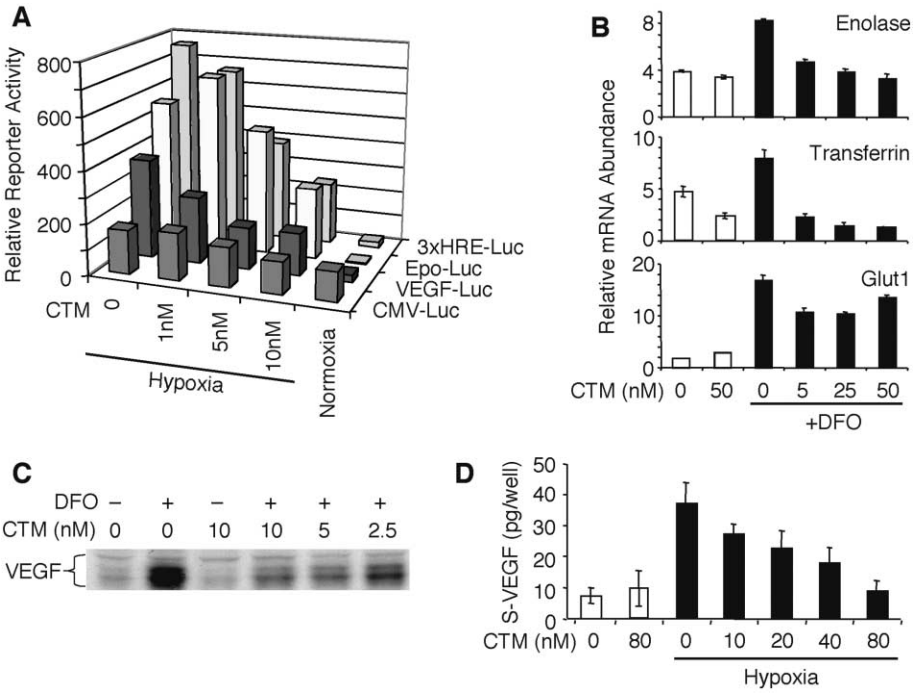

Figure 4. Chetomin attenuates hypoxia-inducible transcription

A: Hypoxia-inducible reporter assays. Hep3B cells were transfected with the indicated hypoxia-responsive reporters (3xHRE-Luc, EPO-Luc, VEGF-Luc) or a constitutive control (CMV-Luc). Reporter activity under normoxic or hypoxic conditions and in the absence or presence of the indicated concentrations of chetomin (CTM) are expressed normalized to an internal control for transcription (β-galactosidase activity).

B: Abundance of hypoxia-inducible mRNA. The abundance of the indicated hypoxia-responsive transcripts under normoxic (open bars) or hypoxia-mimetic conditions (deferoxamine [DFO]; filled bars) was quantified by real-time RT-PCR. The effect of chetomin is expressed as the average of triplicate experiments ± SD.

C and D: Cellular and secreted VEGF abundance. Hep3B cells treated in the absence or presence of chetomin (CTM) and hypoxia or DFO were lysed and immunoblotted for VEGF (**C**), or the abundance of VEGF in the tissue culture supernatant was assayed by ELISA (**D**).

after the final dose, and EPO was immunoprecipitated and then quantified by immunoblot. Animals that were treated acutely with chetomin had a significant decrement in serum EPO levels (Figure 6A). Consistent with these acute effects, animals that were treated for 3 weeks with chetomin (see Figure 7A) had specific decreases in red blood cell counts (Figure 6B).

The effect of acute administration of chetomin on pathological HIF-1 activity was evaluated in mice bearing established HCT116 xenograft tumors. Mice were again treated with either three daily doses of chetomin at 2 mg/kg i.v. or vehicle control. We evaluated the effect of chetomin on the expression of two HIF-1 target genes, glucose transporter 1 (Glut1) and VEGF, by immunohistochemistry and ELISA, respectively. Since oxygenation within tumors is highly heterogeneous, we examined Glut 1 immunoreactivity specifically in perinecrotic areas, where cells are most hypoxic and there is peak hypoxia-driven gene expression (Damert et al., 1997). VEGF levels were determined from standardized tumor lysates. Chetomin was found to acutely attenuate both Glut1 expression (Figure 5C) and tumor VEGF levels (Figure 5D), as biomarkers of HIF-1 activity within tumors.

To directly determine the effect of chetomin on the HIF-1 pathway within tumors, we used in vivo bioluminescence imaging to quantify hypoxia-inducible transcription. We created a hypoxia reporter cell line in which luciferase was expressed under control of the EPO enhancer (HepG2-EPO-Luc). In cell culture, this reporter cell line had >100-fold induction of reporter activity under hypoxic conditions when compared to normoxic conditions (data not shown). To validate the cell line for in vivo assessment of hypoxia-induced transcription, aliquots of the reporter cell line were infected with retroviruses encoding dominant-negative (dnHIF) or dominant-positive (HIF-VP16) mediators of HIF-mediated transcription, as previously described (Kung et al., 2000). When identical numbers of cells were implanted as xenografts in nude mice, bioluminescence was clearly visualized 48 hr after implantation (Figure 6A). Specificity of the reporter activity was validated by the fact that luminescence was attenuated by concomitant expression of dnHIF polypeptide and superactivated by HIF-VP16, a constitutively active allele of HIF-1α. The retroviral vector controls (pMMP and pBP) were comparable to otherwise unmodified reporter cells (Figure 6A). Thus, the luminescent signal emanating from these reporter cells was a reflection of the transcriptional activity of the HIF-1 pathway within these tumors.

To assess the in vivo effect of chetomin on hypoxia-inducible transcription, we innoculated nude mice with hypoxia reporter cell line on the right flank (HepG2-EPO-Luc). As an internal control, a cell line with luciferase constitutively expressed from the CMV promoter was implanted on the left flank (HepG2-CMV-Luc). Mice were imaged 48 hr after implantation to establish baseline reporter activity and were then i.v. injected with either 2 mg/kg chetomin or vehicle control. After two doses, 24 hr after baseline imaging, mice were reimaged (Figure 6B). Total flux of photons through a standardized region of interest drawn around each injection site was determined, and hypoxia-specific reporter activity was derived as the ratio of luminescence from EPO-Luc-containing cells relative to the constitutive internal control (EPO-Luc/CMV-Luc). Hypoxia-specific reporter activity was marginally increased in vehicle-treated mice (+11%, +13%) over the treatment period. In contrast, the hypoxia reporter activity in mice treated with chetomin was reduced by approximately half (−40%, −52%). These results, together with the biomarker studies above, demonstrate that systemic administration of chetomin attenuates both physiological and pathological HIF-mediated gene expression.

In vivo disruption of HIF/p300 interaction

We adapted a previously described method for molecular imaging of protein-protein interactions (Ray et al., 2002) to evaluate

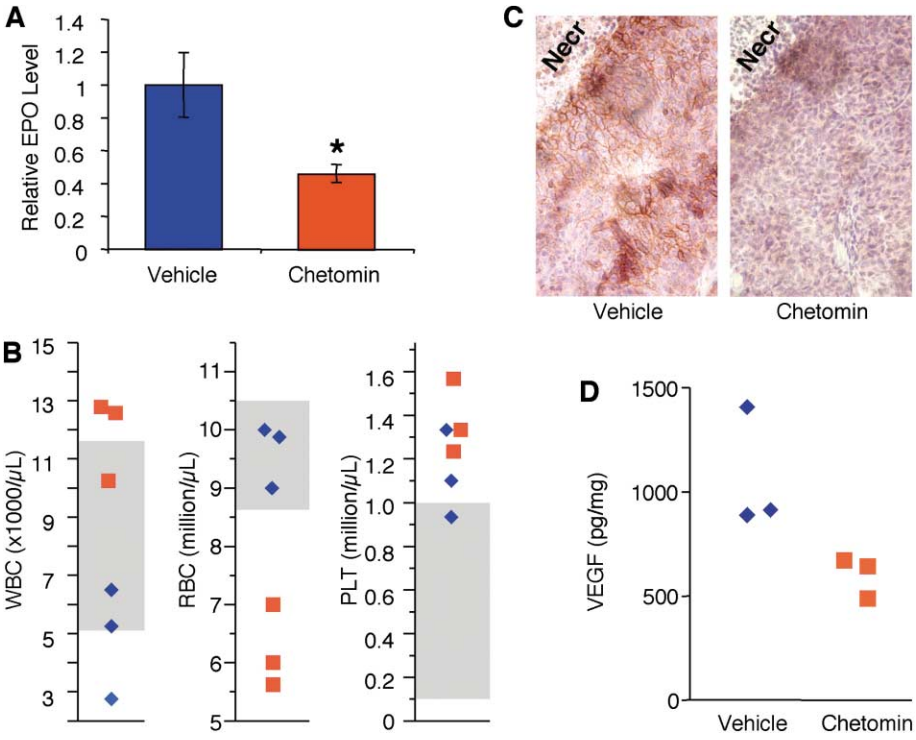

Figure 5. Chetomin attenuates HIF-1 biomarkers in vivo

A: Serum EPO levels in mice treated with 2 mg/kg of chetomin or vehicle control via tail vein, daily for 3 days. Data presented relative to control levels; mean ± SEM; n = 4 in each group; *p < 0.05.

B: Blood counts from individual mice treated 3 weeks with chetomin (red squares) or vehicle control (blue diamonds). See Figure 7A for dosing regimen. Normal range of lab values indicated by gray shading.

C and D: Glut1 immunostaining (**C**) and VEGF levels (**D**) in HCT116 xenograft tumors treated with three daily doses of chetomin at 2 mg/kg or vehicle control. For Glut1 immunostaining (brown), representative areas with comparable localization relative to areas of necrosis (Necr) are shown. VEGF levels are reported as pg of human VEGF per mg of tumor lysate.

the effect of chetomin on the interaction of HIF-1 with p300. As with the cell culture mammalian two-hybrid assays described in Figure 2B, reporter cells were created by cotransfecting plasmids expressing Gal4-TADC and VP16-CH1. The activity of luciferase expressed from a Gal4-Luciferase vector was used as a quantitative measure of this protein-protein interaction (Ray et al., 2002). Control cells were created by expressing the Gal4 DNA binding domain fused directly to VP16 (Gal4-VP16) to constitutively drive expression of Gal4-Luc.

We inoculated mice with two-hybrid reporter cells in the right flank and constitutive control cells in the left flank (Figure 6C). After 24 hr, mice were imaged to determine baseline reporter activity. Animals were then treated with either chetomin (2 mg/kg) i.v. or vehicle control. After three daily doses, mice were reimaged (Figure 6C). In all cases, two-hybrid interaction reporter luminescence was normalized to the control luminescence on the contralateral flank (i.e., to correct for cytotoxic or nonspecific effects), and results are expressed relative to the baseline activity. With this molecular imaging approach, chetomin was found to significantly disrupt the TADC/CH1 protein-protein interaction within tumors in vivo (Figure 6D), as it did in vitro (Figure 2A) and in cell culture (Figures 2B and 2C).

Effects of chetomin on tumor growth

We utilized xenograft tumor models to evaluate the effect of chetomin on tumor growth. HCT116 colon cancer cells were implanted subcutaneously and allowed to grow to approximately 50 mm^3 prior to initiation of therapy. When given at 2 mg/kg, chetomin was found to cause local toxicity at sites of repeated intravenous injection, and this limited the number of doses that could be administered by tail vein injection. As such, treatments were administered by injection through a central venous catheter for the effective lifespan of such catheters (2 weeks), followed by a limited number of tail vein injections (1 week). In comparison to mice treated with vehicle control, 2 mg/kg of chetomin given at the indicated frequency had significant antitumor activity (Figure 7A) without significant effects on body weight over the treatment period (Figure 7B). Necropsy revealed coagulative necrosis at sites of tail vein injection (data not shown), and blood counts revealed anemia and leukocytosis (Figure 5B). We have not been able to determine the cause of the local coagulative necrosis and leukocytosis but suspect that the latter may be a secondary effect of the former. There was no other overt end-organ toxicity in chetomin-treated mice.

When given at a lower dose of 1 mg/kg, the onset of local toxicity at sites of injection was significantly diminished. When chetomin was administered daily at 1 mg/kg i.v., there was likewise significant antitumor efficacy in mice xenografted with PC3 cells (Figure 7C). Histological examination of tumor sections revealed significant necrosis in chetomin-treated tumors in comparison to minimal necrosis in vehicle-treated mice at comparable distances from the tumor surface (Figure 7D). Immunostaining for HIF-induced gene products (e.g., Glut1, VEGF) and vasculature revealed vast regional variability in chetomin-treated tumors and were uninterpretable as to whether they were primary or late downstream treatment effects.

Discussion

Disrupting the ability of tumors to adapt to hypoxia may be an attractive antitumor strategy given the universality of hypoxia in solid tumors. Our prior studies demonstrated that attenuation of the HIF-1 pathway could be achieved through blockade of the interaction of p300/CBP with HIF-1α through the overexpression of a blocking polypeptide in tumor cells (Kung et al., 2000). Here, we describe our efforts to find a small molecule

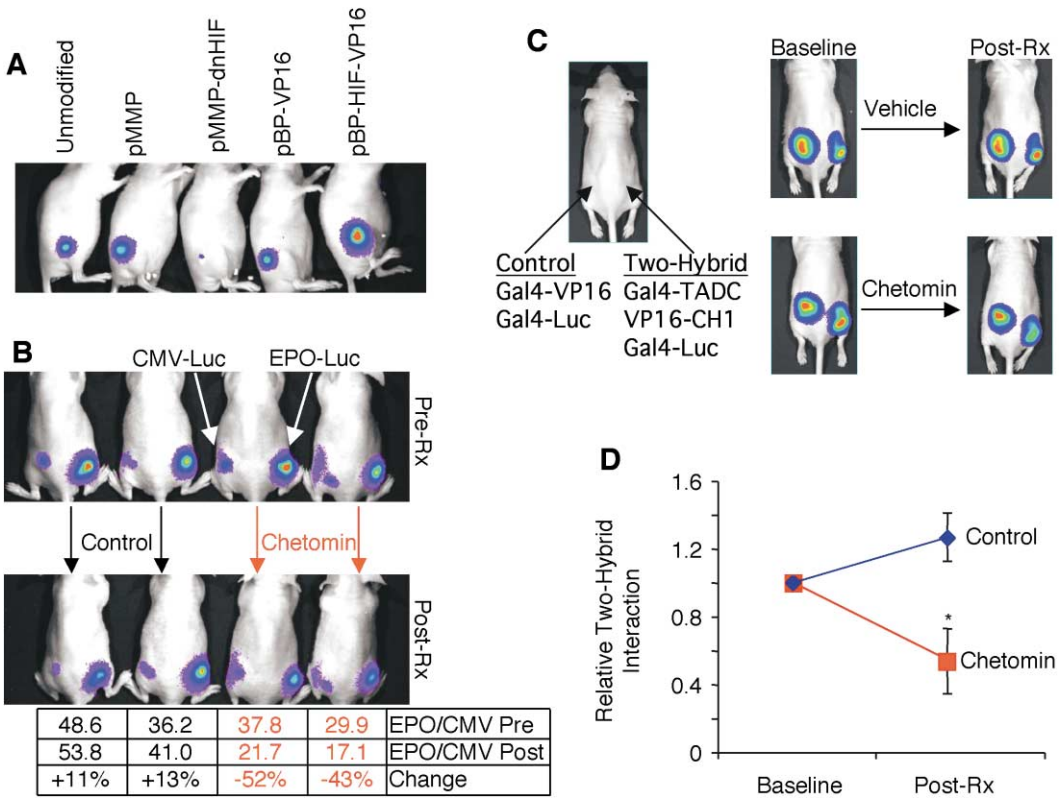

48.6	36.2	37.8	29.9	EPO/CMV Pre
53.8	41.0	21.7	17.1	EPO/CMV Post
+11%	+13%	-52%	-43%	Change

Figure 6. Chetomin disrupts HIF pathway activity in vivo

A: In vivo imaging of HIF-1 activity. HepG2 cells with stably integrated EPO-Luc reporter were implanted without further modification or after infection with retroviruses encoding a dominant-negative HIF polypeptide (pMMP-dnHIF), dominant-positive HIF-1α allele (pBP-HIF-VP16), or controls for retroviral infection (pMMP, pBP). Mice were imaged 48 hr after implantation of cells.

B: In vivo effects of chetomin. Hypoxia reporter cells (EPO-Luc) were implanted on the right flank, and constitutive control cells (CMV-Luc) were implanted on the left flanks of mice. Animals were imaged prior to (Pre-Rx) and after (Post-Rx) i.v. administration of two doses of chetomin (2 mg/kg) or vehicle control. HIF-1-specific activity was determined by calculating the ratio of EPO-Luc/CMV-Luc.

C: In vivo imaging of TADC-CH1 protein-protein interaction. Mice were inoculated with two-hybrid reporter cells in the right flank and constitutive control cells in the left flank. After baseline imaging, mice were treated with two doses of chetomin (2 mg/kg) or vehicle control, followed by reimaging 24 hr after initial imaging.

D: For each animal, TADC-CH1 two-hybrid interaction (right flank) was normalized to the constitutive control (left flank) and expressed relative to the baseline ratio for each animal; mean ± SEM; n = 4; *$p < 0.05$.

capable of blocking this nuclear protein-protein interaction. The primary candidate that emerged from a target-based HTS, chetomin, was found to indeed be able to block the interaction of HIF-1α and HIF-2α with p300 by disrupting the HIF-interacting domain of p300. This resulted in attenuation of hypoxia-inducible transcription in cell culture, as well as in vivo when systemically administered in mice.

While the biomarker analyses (EPO/VEGF/Glut1 levels, in vivo molecular imaging) suggest that chetomin indeed hits its intended target, the HIF pathway and specifically HIF-p300 interaction, in vivo, the exact basis of the downstream antitumor activity requires further investigation. Our attempts to rescue tumors from chetomin by overexpressing HIF-VP16 in tumor cells, as we have previously done (Kung et al., 2000), resulted in only partial rescue of tumor growth (data not shown). One possible explanation for this finding is that systemically administered inhibitors target both tumor and host elements (e.g., stromal cells, endothelial cells). The importance of the stroma in supporting tumor growth is underscored by the fact that a large fraction of VEGF within mouse tumors is actually produced by stromal elements (Fukumura et al., 1998), and furthermore, attenuation of HIF may also have direct effects on endothelial cell viability or function as suggested by recent studies (Sowter et al., 2003; Yamakawa et al., 2003). It is thus possible that, since HIF-VP16 is expressed solely in the tumor cells, partial rescue results from the unimpeded effects of chetomin on host elements. Although the precise function and requirement for the HIF pathway in the tumor and host compartments are active areas of study, the current results with chetomin suggest a therapeutic window for inhibition of HIF function as a therapeutic target.

We demonstrate that the HIF-1 pathway can be attenuated by blocking the function of an associated transcriptional coactivator. This approach does not confer absolute specificity of action, and our results suggest that other CH1-interacting transcriptional pathways are also blocked. Indeed, another possible explanation for partial rescue of tumor growth with HIF-VP16 (see above) is that chetomin may have off-target effects that contribute to antitumor efficacy. However, in our prior studies utilizing a polypeptide to block CH1, the in vivo antitumor effects

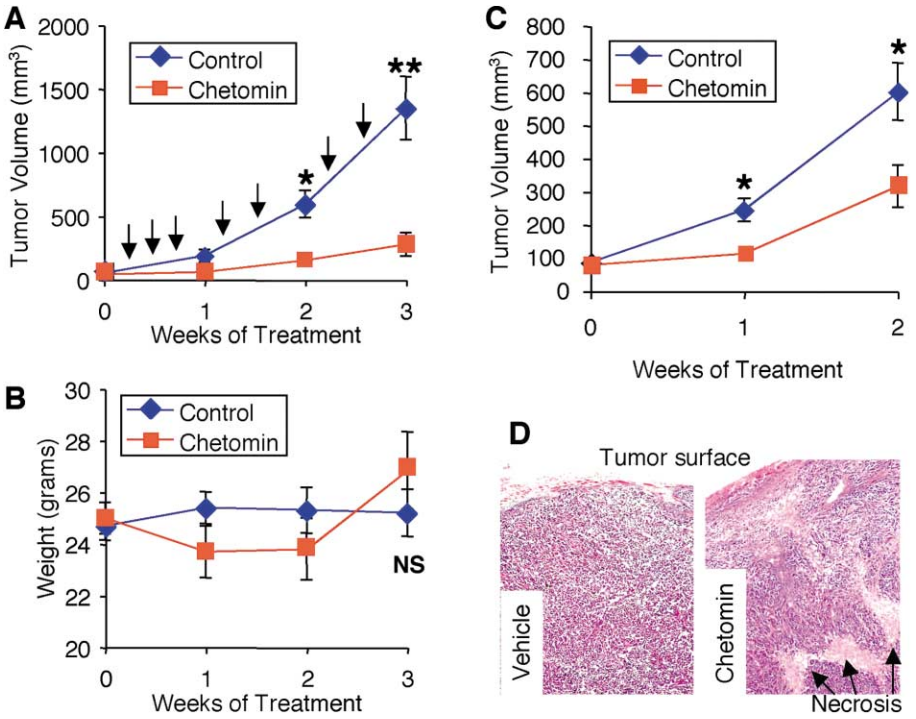

Figure 7. Chetomin attenuates tumor growth in vivo

A and B: Chetomin effects on (**A**) tumor growth and (**B**) body weight in mice with HCT116 xenografts. Animals with established tumors after 1 week of growth were divided into groups treated with 2 mg/kg chetomin i.v. or vehicle control (arrows indicate doses). Data represent means ± SEM; n = 6 per group; *$p < 0.05$; **$p < 0.005$. NS, not significant.

C: Effects of chetomin (1 mg/kg) i.v. daily (5 days/week) or vehicle control on growth of established PC3 xenografts. Data presented as mean ± SEM; n = 10 per group; *$p < 0.05$.

D: Low-power view of H&E-stained tumor sections from PC3 xenografts. The tumor surfaces and areas of necrosis are indicated. The scale is identical in the two panels.

were largely attributable to inhibition of the HIF pathway, since overexpressing HIF-VP16 largely rescued tumor growth (Kung et al., 2000). Our results also demonstrate that chetomin is also not totally nonspecific. That is, cellular transcription is not globally attenuated, as it is with actinomycin D, nor is the function of p300/CBP lost in entirety. Since p300 and CBP are critical coactivators of many transcriptional pathways that are ectopically activated in cancer, this strategy may have broader utility in targeting other transcriptional pathways and transcription factors. Attacking downstream mediators of transcription has the theoretical advantage of targeting common end effectors in the case of pathways where mutations in multiple upstream components could all contribute to ectopic activation, e.g., the WNT pathway (Morin et al., 1997). Recent reports of peptidic (Lau et al., 2000) and small molecule inhibitors (Balasubramanyam et al., 2003) of p300/CBP acetyltransferase activity suggest another method for attacking these coactivators.

There are only a few examples where a signal transduction pathway has been disrupted by small molecule inhibition of a downstream protein-protein interaction (Berg et al., 2002; Lepourcelet et al., 2004). The interaction surface of p300/CBP with HIF-1α is extensive, totaling 3393 Å, and the a priori prediction would be that it would be difficult to find a small molecule capable of blocking this extended protein-protein interaction (Freedman et al., 2002). The mechanism of action in the case of chetomin appears to be disruption of the tertiary structure of CH1. This result suggests that blockade of protein-protein interactions may not require physical allosteric blockade of binding but rather may be accomplished through induction of structural changes of one of the binding partners. The inverse has previously been demonstrated, in which protein structure and function has been restored by small molecule modulation of mutant p53 structure (Foster et al., 1999).

Modern drug discovery is increasingly focused on targeting pathognomonic changes in cancer cells. There are broad classes of targets, however, where selectivity may not result from absolute restriction in expression but rather from differential function in tumor cells in comparison to their normal counterparts. Recent clinical success with bortezomib, an inhibitor of proteosome function, is one such example. The HIF pathway is another example, in that the pathway is present in all cells, but hypoxic tumors may have a heightened dependence upon its function for survival and growth. While further development of chetomin as a therapeutic may be limited by its local toxicity, the results presented herein suggest that the HIF pathway can be attenuated in vivo with a therapeutic window. Additional target-based screens derived from our expanding knowledge of the molecular regulation of the HIF pathway or phenotypic cell-based screens utilizing hypoxia reporter cells (Rapisarda et al., 2002), will hopefully yield additional candidate compounds for development and evaluation as potential clinical therapeutics.

Experimental procedures

Reagents, plasmids, and retroviruses

Except where otherwise noted, all reagents were from Sigma. Mammalian two-hybrid vectors pB42-CH1, pGal4-CAD, pGal4-CAD-C800V, and pGal4-CAD-C800S were kind gifts of L. Eric Huang (National Cancer Institute) (Gu et al., 2001). pcDNA3-HA-HIF-2α was kindly provided by William G. Kaelin, Jr. (Dana-Farber Cancer Institute). All other plasmids and retroviruses have been previously described (Bhattacharya et al., 1999; Kung et al., 2000).

Fermentation and isolation of chetomin

Chetomin was produced by fermentation of *Chaetomium sp.*, followed by extraction and purification by column chromatography. Details are provided in the Supplemental Data at http://www.cancercell.org/cgi/content/full/6/1/33/DC1.

HIF-1/p300 HTS

GST-CH1 was expressed in BL21 pLysS cells (Promega), transformed with pGEX-2T-CH1 (aa 302-423) (Kung et al., 2000), and grown in Luria-Bertani broth media supplemented with 0.1 mM $ZnCl_2$. Expression was induced with 0.4 mM IPTG overnight at 25°C. The bacteria were lysed by sonication in lysis buffer (50 mM Tris 8.0, 150 mM NaCl, 100 μM $ZnCl_2$, 1 mM EDTA, 10 mM $MgCl_2$, 1 mM dithiothreitol (DTT), 0.1% NP40, 50 μg/ml RNAase A, 50 μg/ml DNAase, 10 μM pepstatin, 10 μM leupeptin, and 1 mM Pefabloc [Roche]). After centrifugation, GST-CH1 fusion protein was purified by Glutathione-Sepharose 4B (Amersham) column chromatography according to the manufacturer's instructions. After elution with 50 mM glutathione, fractions with highest protein concentration were pooled and dialyzed overnight at 4°C in 2 liters of 50 mM Tris 8.0, 150 mM NaCl, 100 μM $ZnCl_2$, 1 mM DTT, 0.1% NP40, 10% glycerol, and 0.1 mM Pefabloc. The GST-CH1 protein was filtered and stored at −70°C.

Multiwell plates (Nunc) were coated with streptavidin 1 μg/ml overnight at 4°C in PBS. The plates were washed with 50 mM Tris 8.0, 150 mM NaCl, and 0.05% Tween 20 (TBST). Synthetic N-terminal biotinylated HIF-1α peptide (aa 786-826) was bound in 50 mM Tris 8.0, 150 mM sodium chloride, and 5% bovine serum albumin (assay buffer) for 2 hr at 4°C. The plates were washed with TBST, and 111 pM GST-CH1 was added to the plates in assay buffer with 0.1% Tween 20, 0.5 mM DTT, and 10 μM $ZnCl_2$ and in the presence or absence of compounds for 2 hr at 4°C. The assay plates were washed with TBST, and europium-labeled anti-GST antibody was added in assay buffer with 10 μM $ZnCl_2$ and incubated overnight at 4°C. The plates were washed with TBST, DELFIA enhancement solution (Wallac) was added, and fluorescence was read on a Victor I time-resolved fluorescence detector (Wallac).

HIF-1α/p300 immunoprecipitation

Hep3B cells were treated with 50 nM chetomin or DMSO for 2 hr prior to addition of 125 μM DFO. After 18 hr, cells were scraped into ice-cold PBS, and nuclear extracts were prepared using the NE-PER kit (Pierce) according to the manufacturer's instructions. Standardized aliquots of 10 mg of nuclear extract were incubated with 2 μg each of OZ12 and OZ15 (Arany et al., 1996) HIF-1α-specific monocolonal antibodies for 2 hr at 4°C and immobilized on Protein A/G Sepharose (Amersham) for 1 hr. Beads were extensively washed with 50 mM Tris 8.0, 300 mM NaCl, 1% NP-40, 1 mM DTT, and protease inhibitors (EDTA-free Complete, Roche). Samples were fractionated on SDS-PAGE, transferred to nitrocellulose, and immunoblotted with p300-specific (RW128) or HIF-1α-specific (NB100; Novus) antibodies.

In vitro interaction and cell-based reporter assays

In vitro pull-down, hypoxia reporter, and mammalian two-hybrid assays were performed as previously described (Bhattacharya et al., 1999; Kung et al., 2000). See the Supplemental Data at http://www.cancercell.org/cgi/content/full/6/1/33/DC1 for further details.

NMR spectroscopy

A complex of HIF-1α/CH1 was prepared as previously described (Freedman et al., 2002). CH1 alone was produced in a similar way but was purified by cation exchange (HiTrap SP HP; Amersham) followed by gel filtration (Superdex75; Amersham). Samples were prepared by dissolving 125 μM unlabeled protein in 10 mM deuterated MES (pH 6.0), 90% D2O with or without 100 mM NaCl, 0.1 mM ZnSO4, and 1 mM deuterated DTT. One-dimensional ^{1}H NMR spectra were acquired on a Unity Inova 500 MHz spectrometer (Varian) at 25°C. Data were processed using the program PROSA, and the spectra were displayed using the program XEASY. Chetomin (25 mM) in 100% DMSO was added to protein samples in aqueous solution to final concentrations of 50 μM, 100 μM, and 250 μM. In control experiments, DMSO alone was added to protein samples using volumes that matched each of the chetomin additions (maximum 1% DMSO in each sample). EDTA (1 mM) was added to a protein sample containing 1% DMSO but not chetomin.

Real-time PCR

Hep3B cells were treated with compound or vehicle control for 8 hr prior to induction of hypoxia. Cells were maintained in hypoxia overnight, washed to remove debris, and total RNA was harvested using Trizol reagent (Invitrogen) according to the manufacturer's protocol. Reverse transcription was performed with 2.5 μg of total RNA added to buffer, random hexamers, dNTPs, RNase inhibitor, and reverse transcriptase (TaqMan; Applied Biosystems) according to the manufacturer's instructions. Real-time PCR was then conducted using 5 μl of template according to the manufacturer's instructions (SYBR Green PCR; Applied Biosystems). Reactions were run and analyzed using the 5700 GeneAmp instrument and software (Applied Biosystems).

Immunoblot and ELISA analysis of VEGF

Hep3B cells were treated with compound or vehicle control (DMSO) for 8 hr prior to addition of 125 μM DFO to induce hypoxia response. After 18 hr, cells were lysed in 100 mM Tris-Cl 6.8, 4% SDS, 20% glycerol, and protease inhibitor cocktail. After centrifugation, the protein concentration of the supernatant was determined (BioRad), and 50 μg of each lysate was resolved by SDS-PAGE on a 12% Tris-glycine gel. After transfer to nitrocellulose, immunodetection with anti-VEGF antibody (AB1442; Chemicon) was performed using standard techniques. Tissue culture supernatant levels of VEGF was determined using a VEGF immunoassay (R&D Systems) according to the manufacturer's instructions.

In vivo EPO and VEGF levels, Glut1 immunostain, and blood counts

NCr/Nude mice (Taconic) either with or without HCT116 xenografts were treated for the indicated periods of time with chetomin or vehicle control (10% DMSO, 4.5% dextrose). After humane euthanasia, blood was immediately collected by intracardiac aspiration. For EPO levels, serum was isolated using a serum separator tube (BDBioscience). Serum EPO was immunoprecipitated from 200 μl of serum using a polyclonal anti-mouse EPO antibody (Santa Cruz Biotechnology), followed by immunoblot with a monoclonal antibody (Pharmingen). Relative levels were determined by densitometry. For blood counts, blood was collected in anticoagulant, and complete blood counts were performed by the clinical laboratory. For Glut1 and VEGF determination, tumors were excised, and half of each tumor was fixed in buffered 10% formalin and then immunostained for Glut1 as previously described (Kondo et al., 2002). The other half of each tumor was flash frozen in liquid nitrogen, pulverized to a powder with a mortar and pestle, and lysed in RIPA buffer (150 nM NaCl, 1% NP-40, 0.5% DOC, 0.1% SDS, and 50 mM Tris [pH 7.4]) containing protease inhibitors (Complete, Roche). Standardized aliquots of 0.1 mg of total protein were assayed using an ELISA specific for human VEGF (R&D Systems) according to the manufacturer's instructions.

In vivo imaging and xenografts

HepG2 cells (ATCC) were cotransfected with either EPO-luciferase (EPO-Luc) or CMV-luciferase along with a neomycin phosphotransferase expression vector. G418-resistent colonies were isolated and assayed for responsiveness to hypoxia. A clone of HepG2 with stably integrated EPO-Luc was identified with >100-fold induction in cell culture. For validation, aliquots of this clone were infected with pMMP, pMMP-dnHIF, pBP, or pBP-HIF-VP16 as described previously (Kung et al., 2000). Xenografts were generated by injecting 5×10^6 of the indicated cells subcutaneously in NCr/Nude mice (Taconic). Mice were anesthetized with a mixture of ketamine hydrochloride (150 mg/kg), xylazine (12 mg/kg), and D-luciferin (50 mg/ml) (Xenogen, Alameda, CA) and imaged utilizing the In Vivo Imaging System (IVIS; Xenogen) for a duration of 60–120 s. Mice were allowed to recover under isothermic conditions after imaging. To quantify bioluminescence, identical standardized circular regions of interest (ROI) were positioned to encircle the areas of emission, and the integrated flux of photons through each ROI (photons/s) was determined using the Living Images software package (Xenogen).

For in vivo two-hybrid interaction imaging, reporter cells were created by transfecting HCT116 cells with expression vectors encoding Gal4-TADC, VP16-CH1, and Gal4-Luc, as described in the Supplemental Data at http://www.cancercell.org/cgi/content/full/6/1/33/DC1. Control cells were cotransfected with an expression vector encoding Gal4 DNA binding domain directly fused with the VP16 transactivation domain (Gal4-VP16) along with Gal4-Luc. Four hours after transfection with Lipofectamine 2000 (Invitrogen), 10^7 control cells were injected subcutaneously into the left flank, and 10^7 two-hybrid reporter cells were injected into the right flank. Animals were imaged as described 24 hr after implantation and then divided into cohorts of mice which were treated with two doses of chetomin at 2 mg/kg or vehicle control via tail vein injection (doses separated by 18 hr). Mice were reimaged 6 hr after the second dose (24 hr after first image). The flux of photons through

standardized regions of interest was determined as described above. For each animal, changes in the two-hybrid reporter activity (right flank) were normalized to changes in the control emission (left flank) to correct for nonspecific changes in gene expression or luminescence, and results are expressed relative to the baseline ratio [Relative two-hybrid interaction = $(PostRxFlux_{2hybrid}/BaselineFlux_{2hybrid})/(PostRxFlux_{control}/BaselineFlux_{control})$].

HCT116 and PC3 xenografts were generated by subcutaneous injection of 5×10^6 cells into NCr/Nude mice. Where indicated, mice were purchased with jugular central venous catheters (CVC) in place. After 1 week of growth, mice with measurable tumors were segregated into treatment groups of six to eight animals with unilateral xenografts or five animals with bilateral xenografts. Where indicated, chetomin or vehicle control was administered via CVC for the useable lifespan of the CVC, at which time mice were dosed via tail vein injections. Tumors were measured with calipers, and the tumor volume was calculated as $0.5 \times \text{length} \times \text{width}^2$.

All animal procedures were performed under the auspices of protocols approved by the Dana-Farber Cancer Institutional Animal Care and Use Committee.

Acknowledgments

This work was supported in part by the DFCI-Novartis Drug Discovery Program (A.L.K., D.M.L., M.J.E.), the National Cancer Institute (A.L.K., D.M.L.), the National Heart, Lung, and Blood Institute (S.J.F.), and a Scholar Award from the American Society of Hematology (S.J.F.). We thank Brigitta Liechty and Hans Hofmann for the cultivation of *Chaetomium sp*. and purification of chetomin from fermentation broths and Peter Lassota and Jeffrey Cramer for in vivo pharmacokinetic studies. We thank Christian Guenat and Lukas Oberer for proof of Chetomin structure by NMR and high-resolution mass spectroscopy. We thank Karen Wang for additional mass spectral analyses, Florence Poy for expression and purification of CH1, and Renee Wright for assistance with in vivo studies.

Received: February 10, 2004
Revised: May 21, 2004
Accepted: May 27, 2004
Published: July 19, 2004

References

Arany, Z., Huang, L.E., Eckner, R., Bhattacharya, S., Jiang, C., Goldberg, M.A., Bunn, H.F., and Livingston, D.M. (1996). An essential role for p300/CBP in the cellular response to hypoxia. Proc. Natl. Acad. Sci. USA *93*, 12969–12973.

Balasubramanyam, K., Swaminathan, V., Ranganathan, A., and Kundu, T.K. (2003). Small molecule modulators of histone acetyltransferase p300. J. Biol. Chem. *278*, 19134–19140.

Berg, T., Cohen, S.B., Desharnais, J., Sonderegger, C., Maslyar, D.J., Goldberg, J., Boger, D.L., and Vogt, P.K. (2002). Small-molecule antagonists of Myc/Max dimerization inhibit Myc-induced transformation of chicken embryo fibroblasts. Proc. Natl. Acad. Sci. USA *99*, 3830–3835.

Bhattacharya, S., Eckner, R., Grossman, S., Oldread, E., Arany, Z., D'Andrea, A., and Livingston, D.M. (1996). Cooperation of Stat2 and p300/CBP in signalling induced by interferon-α. Nature *383*, 344–347.

Bhattacharya, S., Michels, C.L., Leung, M.K., Arany, Z.P., Kung, A.L., and Livingston, D.M. (1999). Functional role of p35srj, a novel p300/CBP binding protein, during transactivation by HIF-1. Genes Dev. *13*, 64–75.

Brewer, D., Duncan, J.M., Jerram, W.A., Leach, C.K., Safe, S., Taylor, A., Vining, L.C., Archibald, R.M., Stevenson, R.G., Mirocha, C.J., and Christensen, C.M. (1972). Ovine ill-thrift in Nova Scotia. 5. The production and toxicology of chetomin, a metabolite of chaetomium spp. Can. J. Microbiol. *18*, 1129–1137.

Brown, J.M. (2002). Tumor microenvironment and the response to anticancer therapy. Cancer Biol. Ther. *1*, 453–458.

Carmeliet, P., Dor, Y., Herbert, J.M., Fukumura, D., Brusselmans, K., Dewerchin, M., Neeman, M., Bono, F., Abramovitch, R., Maxwell, P., et al. (1998). Role of HIF-1α in hypoxia-mediated apoptosis, cell proliferation and tumour angiogenesis. Nature *394*, 485–490.

Carrero, P., Okamoto, K., Coumailleau, P., O'Brien, S., Tanaka, H., and Poellinger, L. (2000). Redox-regulated recruitment of the transcriptional coactivators CREB-binding protein and SRC-1 to hypoxia-inducible factor 1α. Mol. Cell. Biol. *20*, 402–415.

Cochran, A.G. (2000). Antagonists of protein-protein interactions. Chem. Biol. *7*, R85–R94.

Damert, A., Machein, M., Breier, G., Fujita, M.Q., Hanahan, D., Risau, W., and Plate, K.H. (1997). Up-regulation of vascular endothelial growth factor expression in a rat glioma is conferred by two distinct hypoxia-driven mechanisms. Cancer Res. *57*, 3860–3864.

Darnell, J.E. (2002). Transcription factors as targets for cancer therapy. Nat. Rev. Cancer *2*, 740–749.

Ema, M., Hirota, K., Mimura, J., Abe, H., Yodoi, J., Sogawa, K., Poellinger, L., and Fujii-Kuriyama, Y. (1999). Molecular mechanisms of transcription activation by HLF and HIF1α in response to hypoxia: their stabilization and redox signal-induced interaction with CBP/p300. EMBO J. *18*, 1905–1914.

Foster, B.A., Coffey, H.A., Morin, M.J., and Rastinejad, F. (1999). Pharmacological rescue of mutant p53 conformation and function. Science *286*, 2507–2510.

Freedman, S.J., Sun, Z.Y., Poy, F., Kung, A.L., Livingston, D.M., Wagner, G., and Eck, M.J. (2002). Structural basis for recruitment of CBP/p300 by hypoxia-inducible factor-1α. Proc. Natl. Acad. Sci. USA *99*, 5367–5372.

Freedman, S.J., Sun, Z.Y., Kung, A.L., France, D.S., Wagner, G., and Eck, M.J. (2003). Structural basis for negative regulation of hypoxia-inducible factor-1α by CITED2. Nat. Struct. Biol. *10*, 504–512.

Fujimoto, H., Sumino, M., Okuyama, E., and Ishibashi, M. (2004). Immunomodulatory constituents from an Ascomycete, Chaetomium seminudum. J. Nat. Prod. *67*, 98–102.

Fukumura, D., Xavier, R., Sugiura, T., Chen, Y., Park, E.C., Lu, N., Selig, M., Nielsen, G., Taksir, T., Jain, R.K., and Seed, B. (1998). Tumor induction of VEGF promoter activity in stromal cells. Cell *94*, 715–725.

Gu, J., Milligan, J., and Huang, L.E. (2001). Molecular mechanism of hypoxia-inducible factor 1α-p300 interaction. A leucine-rich interface regulated by a single cysteine. J. Biol. Chem. *276*, 3550–3554.

Harris, A.L. (2002). Hypoxia—a key regulatory factor in tumour growth. Nat. Rev. Cancer *2*, 38–47.

Hockel, M., and Vaupel, P. (2001). Biological consequences of tumor hypoxia. Semin. Oncol. *28*, 36–41.

Hopfl, G., Wenger, R.H., Ziegler, U., Stallmach, T., Gardelle, O., Achermann, R., Wergin, M., Kaser-Hotz, B., Saunders, H.M., Williams, K.J., et al. (2002). Rescue of hypoxia-inducible factor-1α-deficient tumor growth by wild-type cells is independent of vascular endothelial growth factor. Cancer Res. *62*, 2962–2970.

Huang, L.E., and Bunn, H.F. (2003). Hypoxia-inducible factor and its biomedical relevance. J. Biol. Chem. *278*, 19575–19578.

Huang, L.E., Gu, J., Schau, M., and Bunn, H.F. (1998). Regulation of hypoxia-inducible factor 1α is mediated by an O2-dependent degradation domain via the ubiquitin-proteasome pathway. Proc. Natl. Acad. Sci. USA *95*, 7987–7992.

Hur, E., Kim, H.H., Choi, S.M., Kim, J.H., Yim, S., Kwon, H.J., Choi, Y., Kim, D.K., Lee, M.O., and Park, H. (2002). Reduction of hypoxia-induced transcription through the repression of hypoxia-inducible factor-1α/aryl hydrocarbon receptor nuclear translocator DNA binding by the 90-kDa heat-shock protein inhibitor radicicol. Mol. Pharmacol. *62*, 975–982.

Isaacs, J.S., Jung, Y.J., Mimnaugh, E.G., Martinez, A., Cuttitta, F., and Neckers, L.M. (2002). Hsp90 regulates a von Hippel Lindau-independent hypoxia-inducible factor-1α-degradative pathway. J. Biol. Chem. *277*, 29936–29944.

Ivan, M., Kondo, K., Yang, H., Kim, W., Valiando, J., Ohh, M., Salic, A., Asara, J.M., Lane, W.S., and Kaelin, W.G., Jr. (2001). HIFα targeted for VHL-

mediated destruction by proline hydroxylation: implications for O2 sensing. Science *292*, 464–468.

Jaakkola, P., Mole, D.R., Tian, Y.M., Wilson, M.I., Gielbert, J., Gaskell, S.J., Kriegsheim, A., Hebestreit, H.F., Mukherji, M., Schofield, C.J., et al. (2001). Targeting of HIF-α to the von Hippel-Lindau ubiquitylation complex by O2-regulated prolyl hydroxylation. Science *292*, 468–472.

Kallio, P.J., Wilson, W.J., O'Brien, S., Makino, Y., and Poellinger, L. (1999). Regulation of the hypoxia-inducible transcription factor 1α by the ubiquitin-proteasome pathway. J. Biol. Chem. *274*, 6519–6525.

Kondo, K., Klco, J., Nakamura, E., Lechpammer, M., and Kaelin, W.G., Jr. (2002). Inhibition of HIF is necessary for tumor suppression by the von Hippel-Lindau protein. Cancer Cell *1*, 237–246.

Kung, A.L., Wang, S., Klco, J.M., Kaelin, W.G., and Livingston, D.M. (2000). Suppression of tumor growth through disruption of hypoxia-inducible transcription. Nat. Med. *6*, 1335–1340.

Lando, D., Peet, D.J., Gorman, J.J., Whelan, D.A., Whitelaw, M.L., and Bruick, R.K. (2002). FIH-1 is an asparaginyl hydroxylase enzyme that regulates the transcriptional activity of hypoxia-inducible factor. Genes Dev. *16*, 1466–1471.

Lau, O.D., Kundu, T.K., Soccio, R.E., Ait-Si-Ali, S., Khalil, E.M., Vassilev, A., Wolffe, A.P., Nakatani, Y., Roeder, R.G., and Cole, P.A. (2000). HATs off: selective synthetic inhibitors of the histone acetyltransferases p300 and PCAF. Mol. Cell *5*, 589–595.

Lepourcelet, M., Chen, Y.N., France, D.S., Wang, H., Crews, P., Petersen, F., Bruseo, C., Wood, A.W., and Shivdasani, R.A. (2004). Small-molecule antagonists of the oncogenic Tcf/β-catenin protein complex. Cancer Cell *5*, 91–102.

Mabjeesh, N.J., Post, D.E., Willard, M.T., Kaur, B., Van Meir, E.G., Simons, J.W., and Zhong, H. (2002). Geldanamycin induces degradation of hypoxia-inducible factor 1α protein via the proteosome pathway in prostate cancer cells. Cancer Res. *62*, 2478–2482.

Mabjeesh, N.J., Escuin, D., LaVallee, T.M., Pribluda, V.S., Swartz, G.M., Johnson, M.S., Willard, M.T., Zhong, H., Simons, J.W., and Giannakakou, P. (2003). 2ME2 inhibits tumor growth and angiogenesis by disrupting microtubules and dysregulating HIF. Cancer Cell *3*, 363–375.

Masson, N., Willam, C., Maxwell, P.H., Pugh, C.W., and Ratcliffe, P.J. (2001). Independent function of two destruction domains in hypoxia-inducible factor-α chains activated by prolyl hydroxylation. EMBO J. *20*, 5197–5206.

McInnes, A.G., Taylor, A., and Walter, J.A. (1976). The structure of chetomin. J. Am. Chem. Soc. *98*, 6741.

Mie Lee, Y., Kim, S.H., Kim, H.S., Jin Son, M., Nakajima, H., Jeong Kwon, H., and Kim, K.W. (2003). Inhibition of hypoxia-induced angiogenesis by FK228, a specific histone deacetylase inhibitor, via suppression of HIF-1α activity. Biochem. Biophys. Res. Commun. *300*, 241–246.

Morin, P.J., Sparks, A.B., Korinek, V., Barker, N., Clevers, H., Vogelstein, B., and Kinzler, K.W. (1997). Activation of β-catenin-Tcf signaling in colon cancer by mutations in β-catenin or APC. Science *275*, 1787–1790.

Pugh, C.W., and Ratcliffe, P.J. (2003). Regulation of angiogenesis by hypoxia: role of the HIF system. Nat. Med. *9*, 677–684.

Rapisarda, A., Uranchimeg, B., Scudiero, D.A., Selby, M., Sausville, E.A., Shoemaker, R.H., and Melillo, G. (2002). Identification of small molecule inhibitors of hypoxia-inducible factor 1 transcriptional activation pathway. Cancer Res. *62*, 4316–4324.

Ray, P., Pimenta, H., Paulmurugan, R., Berger, F., Phelps, M.E., Iyer, M., and Gambhir, S.S. (2002). Noninvasive quantitative imaging of protein-protein interactions in living subjects. Proc. Natl. Acad. Sci. USA *99*, 3105–3110.

Ryan, H.E., Lo, J., and Johnson, R.S. (1998). HIF-1α is required for solid tumor formation and embryonic vascularization. EMBO J. *17*, 3005–3015.

Ryan, H.E., Poloni, M., McNulty, W., Elson, D., Gassmann, M., Arbeit, J.M., and Johnson, R.S. (2000). Hypoxia-inducible factor-1α is a positive factor in solid tumor growth. Cancer Res. *60*, 4010–4015.

Sekita, S., Yoshihira, K., Natori, S., Udagawa, S., Muroi, T., Sugiyama, Y., Kurata, H., and Umeda, M. (1981). Mycotoxin production by Chaetomium spp., and related fungi. Can. J. Microbiol. *27*, 766–772.

Semenza, G. (2002). Signal transduction to hypoxia-inducible factor 1. Biochem. Pharmacol. *64*, 993–998.

Sowter, H.M., Raval, R.R., Moore, J.W., Ratcliffe, P.J., and Harris, A.L. (2003). Predominant role of hypoxia-inducible transcription factor (Hif)-1α versus Hif-2α in regulation of the transcriptional response to hypoxia. Cancer Res. *63*, 6130–6134.

Vaupel, P., Thews, O., Kelleher, D.K., and Hoeckel, M. (1998). Current status of knowledge and critical issues in tumor oxygenation. Results from 25 years research in tumor pathophysiology. Adv. Exp. Med. Biol. *454*, 591–602.

von Pawel, J., von Roemeling, R., Gatzemeier, U., Boyer, M., Elisson, L.O., Clark, P., Talbot, D., Rey, A., Butler, T.W., Hirsh, V., et al. (2000). Tirapazamine plus cisplatin versus cisplatin in advanced non-small-cell lung cancer: A report of the international CATAPULT I study group. Cisplatin and Tirapazamine in subjects with advanced previously untreated non-small-cell lung tumors. J. Clin. Oncol. *18*, 1351–1359.

Yamakawa, M., Liu, L.X., Date, T., Belanger, A.J., Vincent, K.A., Akita, G.Y., Kuriyama, T., Cheng, S.H., Gregory, R.J., and Jiang, C. (2003). Hypoxia-inducible factor-1 mediates activation of cultured vascular endothelial cells by inducing multiple angiogenic factors. Circ. Res. *93*, 664–673.

Zhang, J.H., Chung, T.D., and Oldenburg, K.R. (1999). A simple statistical parameter for use in evaluation and validation of high throughput screening assays. J. Biomol. Screen. *4*, 67–73.

Zhong, H., De Marzo, A.M., Laughner, E., Lim, M., Hilton, D.A., Zagzag, D., Buechler, P., Isaacs, W.B., Semenza, G.L., and Simons, J.W. (1999). Overexpression of hypoxia-inducible factor 1α in common human cancers and their metastases. Cancer Res. *59*, 5830–5835.